

Evidence of non-degenerated, non-reciprocal and ultra-fast spin-waves in the canted antiferromagnet $\alpha\text{-Fe}_2\text{O}_3$

A. El Kanj¹, O. Gomonay², I. Boventer¹, P. Bortolotti¹, V. Cros¹, A. Anane¹, R. Lebrun^{1,*}

¹ *Unité Mixte de Physique, CNRS, Thales, Université Paris-Saclay, 91191 Palaiseau, France*

² *Institute of Physics, Johannes Gutenberg-University Mainz, 55128 Mainz, Germany*

*Corresponding author: romain.lebrun@cnrs-thales.fr

Abstract

Spin-waves in antiferromagnets hold the prospects for the development of faster, less power-hungry electronics, as well as new physics based on spin-superfluids and coherent magnon-condensates. For both these perspectives, addressing electrically coherent antiferromagnetic spin-waves is of importance, a prerequisite that has so far been elusive, because unlike ferromagnets, antiferromagnets couple weakly to radiofrequency fields. Here, we demonstrate the electrical detection of ultra-fast non-reciprocal spin-waves in the dipolar-exchange regime of a canted antiferromagnet. Using time-of-flight spin-wave spectroscopy on hematite ($\alpha\text{-Fe}_2\text{O}_3$), we find that the magnon wave packets can propagate as fast as 30 km/s for reciprocal bulk spin-wave modes and up to 10 km/s for surface-spin waves propagating parallel to the antiferromagnetic Néel vector. The electrical detection of coherent non-reciprocal antiferromagnetic spin waves holds makes hematite a versatile platform where most of the magnonic concepts developed for ferromagnet can be adapted paving the way for the development antiferromagnetic and altermagnet-based magnonic devices.

Introduction

Spin wave dynamics in antiferromagnets holds the prospect of magnonic devices operating at the sub-THz frequencies(1–3) with large group velocity (> 10 km/s) by benefiting from the strong exchange field and quadratic spin-wave dispersion [4,5]. In this context, antiferromagnetic spin-waves in the long and short (including dipole-exchange modes) wave-length limits have been extensively investigated theoretically already some decades ago(6–9). For magnonic devices, one of the most basic actions to be realized is to be able to electrically excite and detect the corresponding fast spin waves. However, up to now, there are no experimental observations of propagating properties of spin waves in AFMs, both in direct and reciprocal space. Indeed, contrary to their counterparts in ferromagnets, in which large stray fields allow to detect inductively the spin wave dynamics relatively straightforwardly, such dipolar fields are zero or largely negligible in antiferromagnets. Beyond their key role in spin wave detection, the non-compensated dipolar fields also provide some of the unique features such as non-reciprocity, magneto-static spin-waves(10, 11), Bose-Einstein condensation(12, 13)) of conventional ferromagnet-based magnonic devices. Due to the bulk Dzyaloshinskii-Moriya interaction(14, 15), canted antiferromagnets are anticipated to present more pronounced dipole-exchange spin-wave modes in the small wave vector \mathbf{k} region (< 6 rad/ μm)(16–19) as required to facilitate their observations using standard inductive detection. Recently, many of these canted antiferromagnet materials, such as hematite and orthoferrites, have also been identified as altermagnets(20, 21), a new class of magnetic materials with opposite spin-sub-lattices, a nearly vanishing compensated magnetic order but at the same time a broken T-symmetry leading to spin-splitting in the momentum space. Such a lifted degeneracy of the electronic spin and magnon band structures shall enable to open to antiferromagnets, the same rich physics of spin current transport and spin wave dynamics(22) than in ferromagnets(23). In this sense, insulating canted antiferromagnets such as hematite, that will be studied here or orthoferrites, which can possess resonance frequencies ranging from 10 to 600 GHz(24–26), DMI fields from 1 to 20 T(27), and low magnetic damping(25, 28, 29), are thus prime candidates to develop the field of antiferromagnetic and alter-magnonics.

In this article, we successfully identify magneto-static spin-waves for low \mathbf{k} vector (0.1 – 2.3 rad/ μm) in hematite ($\alpha\text{-Fe}_2\text{O}_3$). To this aim, we have used spin-wave spectroscopy between two transducer antennas allowing us to detect these AFM spin waves after propagating on a distance of more than 10 μm . Using time of flight spin-wave spectroscopy(30), we evidence the presence of different spin-wave packets with very large group velocities ranging from 5 to 30 km/s. In addition, we report a strongly lifted degeneracy of the bulk spin-wave band for \mathbf{k} perpendicular (\perp) or parallel (\parallel) to the antiferromagnetic order \mathbf{n} , with a separation larger than 1 GHz at $k = 0.6$ rad/ μm . Lastly,

we demonstrate clearly the non-reciprocal character of spin-wave modes for $\mathbf{k} \perp \mathbf{n}$, a highly interesting feature for the development of antiferromagnetic magnonics.

Results and discussions

Lifting of magnon degeneracy in canted antiferromagnets

We excite and detect propagating spin waves in c-plane oriented single crystals of the canted antiferromagnet $\alpha\text{-Fe}_2\text{O}_3$ (14, 31, 32) by means of propagative spin wave spectroscopy(33) (cf. **Fig. 1 (a)**). First we measure with a Vector Network Analyzer (VNA) the transmission parameter L_{21} between two inductive antennas that predominantly excite spin-wave with \mathbf{k} vector of $0.6 \text{ rad}/\mu\text{m}$ (see more details in **Suppl. Mat. 1-3**(34)). We succeed in detecting spin-wave propagation for distances as large as $20 \mu\text{m}$. Such a long-distance coherent transport of antiferromagnetic spin-waves is in line with the recently reported micrometer-long magnon spin-diffusion length and the ultra-low magnetic damping of hematite(28). Due to the small canted moment \mathbf{m} of $\alpha\text{-Fe}_2\text{O}_3$ ($\mathbf{M}_s \approx 3 \text{ emu}/\text{cm}^3$ (31)), the direction of the antiferromagnetic order \mathbf{n} can be oriented perpendicular to the applied field \mathbf{H} with fields as low as 50 mT(31). Indeed, hematite is one of the rare easy-plane antiferromagnet and we specifically chose the sample to have magnetic easy-plane parallel to the surface. This property allows us to investigate spin-wave propagation for $\mathbf{H} // \mathbf{m} \perp \mathbf{n}$, either parallel or perpendicular to the spin-wave vector \mathbf{k} . As described here after, these measurements lead to the observation of strikingly different behaviors for $\mathbf{n} // \mathbf{k}$ and $\mathbf{n} \perp \mathbf{k}$. First, for $\mathbf{n} \perp \mathbf{k}$ (i.e. $\mathbf{H} // \mathbf{k}$), we observe as shown in **Fig. 1 (b)** two close spin-wave branches, around 19 GHz at 150 mT. This could be associated to slightly non uniform anisotropies of the sample(28, 35). For $\mathbf{n} // \mathbf{k}$ (i.e. $\mathbf{H} \perp \mathbf{k}$), we observe a main spin-wave mode (blue line) as shown in **Fig. 1(a)** together several spin-wave branches a few GHz higher in frequency (orange and green lines). These features could indicate the presence of magneto-static modes(16, 19, 28, 36), and we will discuss later how to identify them. It is to be noticed that the lowest spin-wave branches (blue branch) for $\mathbf{H} \perp \mathbf{k}$ follows a similar frequency dispersion as for $\mathbf{H} // \mathbf{k}$, but is always higher in frequency by about 1 GHz. We also see that the signal amplitude strongly varies below 50 mT, because, as mentioned above, of the reorientation of the Néel vector \mathbf{n} and canted moment \mathbf{m} (28, 37) in this low field range.

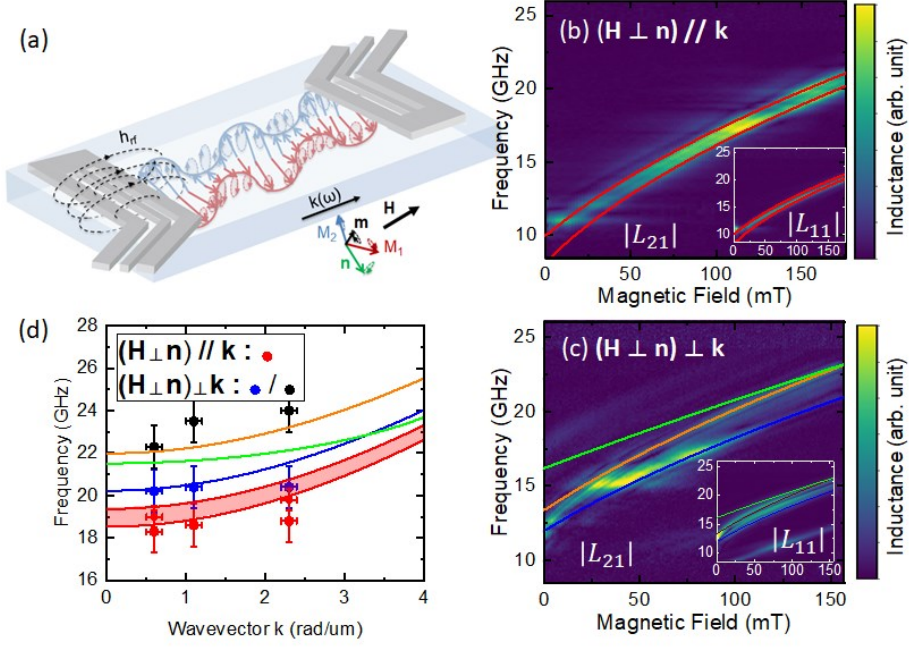


Figure 1. Spin-wave transport in the canted antiferromagnet $\alpha\text{-Fe}_2\text{O}_3$. (a) Schematics of the setup. (b-c) Spin wave transmission measurement showing the transmitted amplitude $|L_{21}|$ for $(\mathbf{H} \perp \mathbf{n}) // \mathbf{k}$ and $(\mathbf{H} \perp \mathbf{n}) \perp \mathbf{k}$ at $\mathbf{k} \approx 0.6$ rad/ μm . (Red and blue lines correspond to fits using the theoretical bulk spin-wave equations for $\mathbf{k} // \mathbf{n}$ and $\mathbf{k} \perp \mathbf{n}$. Orange and green lines respectively correspond to a modelling of the high-frequency spin-wave branch for $\mathbf{k} // \mathbf{n}$ assuming a bulk or a surface mode (see **Suppl. Mat. 7** and Refs. (16, 17, 19)). (d) Magnon branch dispersion for $\mathbf{k} // \mathbf{n}$ and $\mathbf{k} \perp \mathbf{n}$ at a magnetic field of 140 mT. (Red and blue lines correspond to the theoretical bulk spin-wave branches $\mathbf{k} // \mathbf{n}$ and $\mathbf{k} \perp \mathbf{n}$ using the fitting in magnetic field).

To understand the origin of this anisotropic magnon transport, we measure the spin-wave dispersion for $\mathbf{k} \perp \mathbf{n}$ (black and blue points in **Fig. 1 (d)**) and $\mathbf{k} // \mathbf{n}$ (red points in **Fig. 1 (d)**) by performing spin-wave spectroscopy at different \mathbf{k} vectors using several transducer designs (see **Suppl. Mat 1(34)**). We clearly observe the persistence of well-separated magnon branches for the two configurations, with always higher frequencies for $\mathbf{k} // \mathbf{n}$ (see **Suppl. Mat 5(34)**). Indeed such a lifted degeneracy of the magnon dispersion is not expected from the standard degenerated linear dispersion reported for antiferromagnets. To go beyond, other regimes should be considered, such as the dipole-exchange regime of canted antiferromagnets, which in our knowledge has not been yet explored experimentally. As for the difference in spin-wave frequency between the two configurations $\mathbf{k} \perp \mathbf{n}$ and $\mathbf{k} // \mathbf{n}$, some theoretical models(16, 17) do predict that the bulk spin-wave dispersion should vary between these two cases. The refined expression of the bulk spin-wave bands (see **Suppl. Mat 7(34)**) in the dipole-exchange regime leads to a frequency difference $\Delta f_{SW} = f_{\mathbf{k} // \mathbf{n}} - f_{\mathbf{k} \perp \mathbf{n}} = \sqrt{f_{10}^2 + \frac{4\pi M_s}{H_{ex}} \left(\frac{\gamma}{2\pi}\right)^2 (H + H_{DMI})^2} - f_{10} \left(1 + \frac{4\pi M_s}{H_{ex}}\right)$ with f_{10} the frequency gap for the lowest magnon mode(35, 38), γ is gyromagnetic ratio, H_{ex} is exchange field and H_{DMI} is the Dzyaloshinskii-Moriya field. Using the standard values of hematite, we estimate $\Delta f_{SW} \approx 0.5 - 1$ GHz for small \mathbf{k} vectors (10 rad/ μm) which agrees with the observation

that the spin-wave frequencies are lower for $\mathbf{k} \parallel \mathbf{n}$ than for $\mathbf{k} \perp \mathbf{n}$. We can fit the frequency of the bulk spin-wave modes versus fields for these two configurations (see blue and red lines in **Fig. 1 (b-c)**). This result evidences the importance of magneto-static interaction in the spin-wave dynamics of canted antiferromagnets at small \mathbf{k} vectors ($< 10 \text{ rad}/\mu\text{m}$). However, these models cannot explain the presence of the higher frequency spin-wave branches present for $\mathbf{k} \parallel \mathbf{n}$.

Time of flight of surface and bulk antiferromagnetic spin-waves

In order to get more insights about the properties of these propagating AFM spin-waves, we analyze in more details their amplitude and their phase for $\mathbf{k} \parallel \mathbf{n}$ and $\mathbf{k} \perp \mathbf{n}$. We restrict our analysis for magnetic fields above 50 mT to ensure that the Néel vector \mathbf{n} is always strictly perpendicular to the \mathbf{H} . In **Fig. 2 (a)**, we present the imaginary part of the transmitted spin-wave spectra L_{12} for $\mathbf{k} \perp \mathbf{n}$. As shown in **Fig. 2(b)**, we observe the expected oscillatory behavior to the phase delay $\varphi = kD_{ant}$ (with D_{ant} the distance between the two transducer antennae) accumulated by the spin wave during its propagation. From these oscillations, the spin-wave group velocity $v_g = \frac{\partial f}{\partial k} \sim D_{ant} \Delta f$ can be extracted from the periodicity of phase oscillations Δf . However as shown in the black curve of **Fig. 2 (b)**, the envelop of the signal shows the presence of more than one spin-wave packet. Those are due to both wide k -bandwidth of our antenna ($\partial k \approx 0.2 - 1 \text{ rad}/\mu\text{m}$, see **Suppl. Mat. 1(34)**), and potentially to propagating spin-waves with non-uniform thickness profile in our $500 \mu\text{m}$ thick film. To access the group velocity of each spin-wave packets, we perform time gating VNA measurements⁽³⁰⁾ with different intervals (see **Suppl. Mat 4(34)**). As shown in **Fig. 2(b)**, we detect the main (and fastest) spin-wave packets in less than 1 ns of travelling time for a distance of $20 \mu\text{m}$ between the antennas, indicating a group velocity $> 20 \text{ km/s}$. Note that this value is compatible with the group velocity that can be extracted from the phase oscillations Δf in **Fig. 2 (c)**, that lies an average value around 30 km/s over the measured field range. We emphasize that group velocities of such amplitude represents a record velocity for spin-waves in a magnonic device.

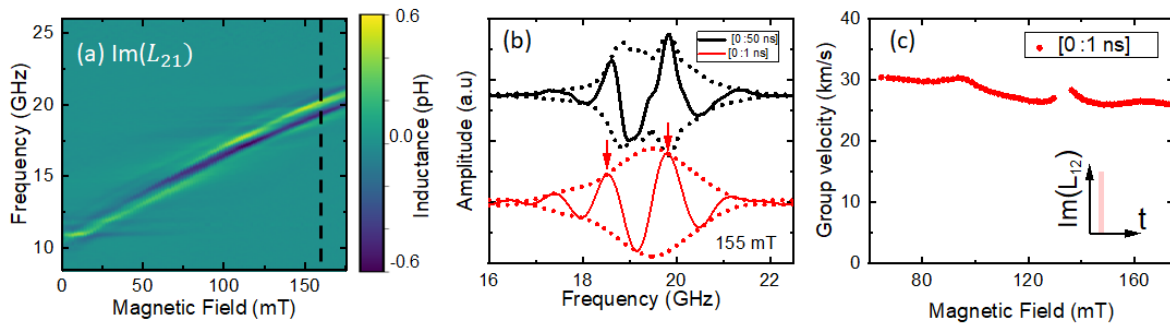


Figure 2. Ultra-fast antiferromagnetic spin-waves for $\mathbf{k} \perp \mathbf{n}$ revealed by time gated VNA measurements. (a) Imaginary part of the transmitted spin-wave $\text{Im}(L_{12})$ as a function of field without time gating. (b) Example of $\text{Im}(L_{12})$ spectra of the full spin-wave signals (time gate of $[0:50 \text{ ns}]$, black) and of the main spin-wave packet (time gate of $[0:1 \text{ ns}]$, red) for $H = 155 \text{ mT}$, indicating a spin-wave group velocity $> 20 \text{ km/s}$. No spin-wave signal is detected after

10 ns. (c) Group velocity of the main spin-wave packet for a time gating of [0:1 ns]. Dotted lines correspond to the signal envelopes. The antenna show a k selectivity centered around $0.6 \text{ rad}/\mu\text{m}$ (see design in Methods).

Contrary to ferromagnets in which the group velocity at small \mathbf{k} scales with the magnetization saturation M_s (39), the group velocity v_g in both collinear and canted antiferromagnets is proportional to H_{ex} (40). Thus, in antiferromagnets, it results that the group velocity can reach tens of km/s as observed in the present work(4), or that domain-wall velocity can be a few km/s as in orthoferrites(5). Note that the observed large spin-wave velocity is also in agreement with the value estimated from the experimental slope of the spin-wave dispersion $\frac{\partial f}{\partial k}$ presented in **Fig. 1 (d)**, which also correspond to spin-wave velocity larger than 10 km/s.

In **Fig. 3**, we present the spin-wave propagating properties in the geometry $\mathbf{k} // \mathbf{n}$. As mentioned before, spin-wave branches separated by a few GHz can be observed in this case. Whilst the first one can be associated to bulk-spin-wave, the higher frequency ones could correspond to the predicted surface spin-wave modes or hybrid surface-bulk modes(19, 35, 36, 41) (see **Suppl. Mat 7**(34)). In **Fig. 3**, we thus present time gating measurements to independently access these different spin-waves modes. As for the configuration $\mathbf{k} \perp \mathbf{n}$, we observe that the first (and fastest) spin-wave packet travels in less than 1 ns and exhibit a group velocity of about 30 km/s (see **Fig. 3 (c)**). It slightly increases with field, leading to larger phase oscillations Δf that become difficult to extract above 120 mT. Surprisingly, the higher frequency spin-wave modes (see blue curves in **Fig. 3(b-c)**) propagates more slowly but still travel in less than 10 ns, having group velocities still around 10 km/s.

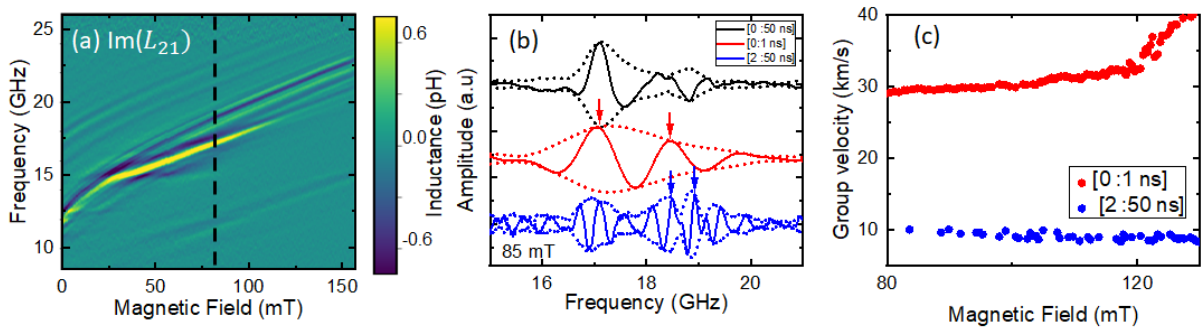


Figure 3. Ultra-fast antiferromagnetic spin-waves for $\mathbf{k} // \mathbf{n}$. (a) Imaginary part of the transmitted spin-wave $\text{Im}(L_{21})$. (b) Exemplary spectra of $\text{Im}(L_{12})$ for $H = 105 \text{ mT}$ for different time gating, [0:50 ns]: full spin-wave signals (black), [0:1 ns]: first spin-wave packet (red), [2:50 ns]: secondary spin-wave packets (blue). Dotted lines correspond to the signal envelopes. (c) Group velocity of the different spin-wave packets. The antenna show a k selectivity centered around $0.6 \text{ rad}/\mu\text{m}$ (see design in Methods).

Non-reciprocal spin-wave transport

Finally, we investigate the potential non-reciprocity of the spin-wave packets for $\mathbf{k} // \mathbf{n}$. Such non-reciprocal behavior which is a key properties for many spin-wave analog devices e.g. circulator, has been widely studied in ferromagnets(42) but up to our

knowledge only predicted in antiferromagnets(7, 8). In **Fig. 4 (a-b)**, we present the amplitude of the transmitted spin-wave packets $|L_{21}|$ for positive and negative fields respectively. We use a time gating of [2:50 ns] to select the high-frequency spin-wave modes (see **Fig. 3 (a)**). As seen in **Fig. 4 (c)**, we do not observe a sizeable frequency shift between positive and negative magnetic fields. However, as far as the spin-wave amplitude is concerned, we find a clear non-reciprocity for two out of the three spin-wave modes. As shown in **Fig. 4 (d)**, we observe for negative magnetic fields a reduction by about a factor 2 of the red mode and even the absence of the blue mode. This non-reciprocal behavior is confirmed by measuring different amplitudes for $|L_{21}|$ and $|L_{12}|$ parameters (see **Suppl. Mat. 6(34)**). These results are signatures of surface spin wave modes propagating with opposite directions at the two surfaces of the sample for $\mathbf{k} \parallel \mathbf{n}$, which are expected also in case of an antiferromagnet(7, 8, 19). On the contrary, for $\mathbf{k} \perp \mathbf{n}$, we measure similar spin-wave amplitudes for the different spin-wave packets between positive and negative fields, and between L_{12} and L_{21} parameters (see **Suppl. Mat. 7(34)**), indicating a reciprocal in this configuration(7, 8). Understanding more in details the symmetry of these spin-waves and how they decay within the AFM thickness remains however to be further theoretically investigated using either the canted antiferromagnet (see **Suppl. Mat. 7(34)**) or altermagnet formalism.

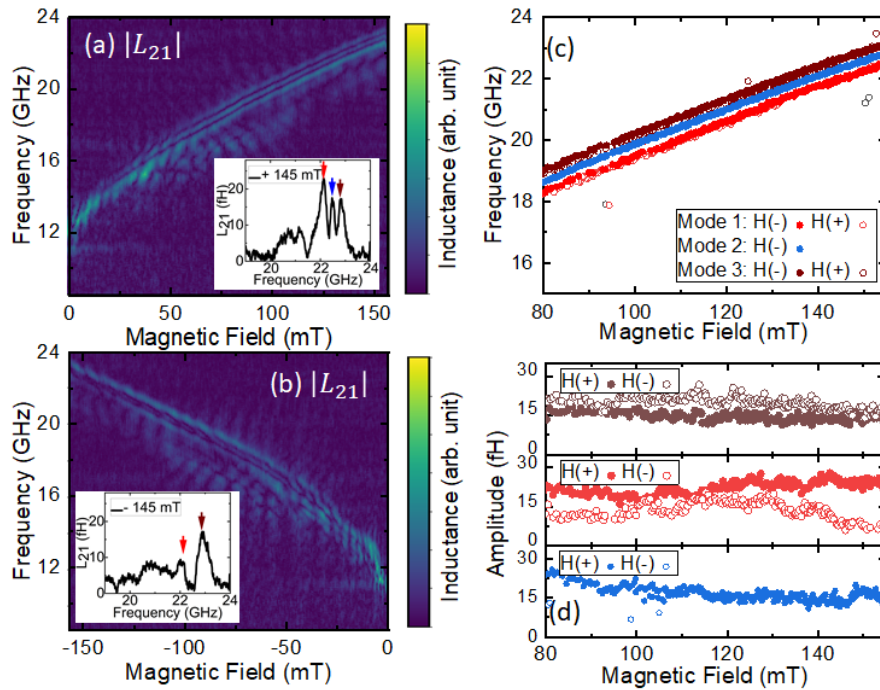


Figure 4. Non-reciprocal spin-wave for $\mathbf{k} \parallel \mathbf{n}$. (a-b) Absolute value of the transmitted spin-wave spectra $|L_{12}|$ with a time gating of [2:50 ns]. Insets shows exemplary spectra for H respectively of $+145$ mT and -145 mT. Arrows indicates the position of the 3 different modes. (c) Frequency and (d) amplitude of the three main spin-wave modes for negative and positive fields.

Discussion

We thus electrically detect the presence of non-degenerated and non-reciprocal spin-waves in the dipolar-exchange regime of a canted antiferromagnet, with record group velocities (of about 30 km/s) and propagation distances up to 20 μm . We can well model the presence of a bulk spin-wave frequency band of a few GHz with lifted degeneracy for $\mathbf{k} \perp \mathbf{n}$ and $\mathbf{k} // \mathbf{n}$, which is anticipated to be a generic feature for canted antiferromagnets at low \mathbf{k} vectors. Furthermore, for $\mathbf{k} // \mathbf{n}$, we observe the co-existence of non-reciprocal with reciprocal spin-wave modes in **Fig. 4**. This non-reciprocal behavior is even enhanced at larger \mathbf{k} (see **Suppl. Mat 6(34)**). Without considering coupling between surface and bulk modes, we can theoretically determine the frequency of the antiferromagnetic surface spin-wave modes to be $f_{sur} = \frac{f_{10}^2 + (\frac{ck}{2\pi})^2}{\frac{\gamma}{\pi}(H + H_{DMI})} + \frac{\gamma}{4\pi} \left(1 + \frac{4\pi M_s}{H_{ex}}\right) (H + H_{DMI})$. Using the material parameters of hematite, we would thus expect spin-wave surface modes at around 32 GHz at 100 mT for $k \approx 0.6 \text{ rad}/\mu\text{m}$. This value is definitively larger than our experimental observations shown in **Fig. 4**, and furthermore the required stability conditions to be localized on the surfaces are not fulfilled (See **Suppl. Mat. 7(34)**). Hence, the frequency of stable surface modes at around 20 GHz can only be fitted with an unrealistic phenomenological effective DMI field ($H_{DMI} \approx 1.3 \text{ T}$, see black lines in **Fig. 1 (b)**). However, similarly to what happen in thick ferromagnets(41), bulk and surface spin-waves can also strongly hybridize in a single crystal. This could thus explain the presence of intermediate frequency spin-wave mode with non-reciprocal spin-wave behavior as observed here. Overall, our findings can only partially be modelled with a standard theory of antiferromagnetic spin-waves (developed in more detailed in **Suppl. Mat 7(34)**). Thus, further theory works would require to investigate in more details the mode interaction and the hybridization depending on the system geometry(16, 17, 19), together with the altermagnetic character of $\alpha\text{-Fe}_2\text{O}_3$ (20, 21, 23). Given the low magnetic damping of other few orthoferrites, the material class of canted antiferromagnets demonstrate all its potentials for establishing a new research field around antiferromagnetic and altermagnonics, with a lot of opportunities for high frequency magnonics.

Note: In the preparation of this manuscript, we became aware of two recent works on spin-wave spectroscopy in hematite in which the authors also observed large group velocities of tens of km/s and long propagation distances(43, 44). Our work evidences that, due to the presence of Dzyaloshinskii-Moriya field, the spin-wave dispersion in this canted antiferromagnet or altermagnet is non-trivial compared to the standard description of an antiferromagnet, being strongly non-degenerated due to magneto-static interaction at small \mathbf{k} vectors, and can show reciprocal and non-reciprocal behaviors.

Acknowledgements

Financial supports from the Horizon 2020 Framework Programme of the European Commission under FET-Open grant agreement No. 863155 (s-Nebula), under FET-Open grant agreement No. 964931 (TSAR) and under the ITN Grant agreement ID 861300 (COMRAD) are acknowledged. The authors also acknowledge support from the ANR TRAPIST (ANR-21-CE24-0011).

References

1. T. Kampfrath *et al.*, *Nat. Photonics*. **5**, 31–34 (2011).
2. J. Li *et al.*, *Nature*, 1–5 (2020).
3. P. Vaidya *et al.*, *Science*. **368**, 160–165 (2020).
4. J. R. Hortensius *et al.*, *Nat. Phys.* **17**, 1001–1006 (2021).
5. V. G. Bar'yakhtar, B. A. Ivanov, M. V. Chetkin, *Sov. Phys. Uspekhi*. **28**, 563–588 (1985).
6. R. E. Camley, *Phys. Rev. Lett.* **45**, 283–286 (1980).
7. B. Lüthi, D. L. Mills, R. E. Camley, *Phys. Rev. B*. **28**, 1475–1479 (1983).
8. B. Lüthi, R. Hock, *J. Magn. Magn. Mater.* **38**, 264–268 (1983).
9. R. L. Stamps, R. E. Camley, *J. Appl. Phys.* **56**, 3497–3502 (1984).
10. B. A. Kalinikos, A. N. Slavin, *J. Phys. C Solid State Phys.* **19**, 7013–7033 (1986).
11. J. R. Eshbach, R. W. Damon, *Phys. Rev.* **118**, 1208–1210 (1960).
12. S. O. Demokritov *et al.*, *Nature*. **443**, 430–433 (2006).
13. B. Divinskiy *et al.*, *Nat. Commun.* **12**, 6541 (2021).
14. T. Moriya, *Phys. Rev.* **120**, 91–98 (1960).
15. I. Dzyaloshinsky, *J. Phys. Chem. Solids*. **4**, 241–255 (1958).
16. W. Jantz, W. Wettling, *Appl. Phys.* **15**, 399–407 (1978).
17. V. I. Ozhogin, *JETP Lett.* **21**.
18. R. Orbach, *Phys. Rev.* **115**, 1189–1193 (1959).
19. V. V. Tarasenko, V. D. Kharitonov, *JETP Lett.* **33** (1971).
20. L. Šmejkal, J. Sinova, T. Jungwirth, *Phys. Rev. X*. **12**, 031042 (2022).
21. L. Šmejkal, J. Sinova, T. Jungwirth, *ArXiv210505820 Cond-Mat* (2021).
22. L. Šmejkal *et al.*, Chiral magnons in altermagnetic RuO₂ (2022), , doi:10.48550/arXiv.2211.13806.
23. L. Šmejkal, J. Sinova, T. Jungwirth, *Phys. Rev. X*. **12**, 040501 (2022).
24. M. Białek, A. Magrez, A. Murk, J.-Ph. Ansermet, *Phys. Rev. B*. **97**, 054410 (2018).
25. S. Das *et al.*, *Nat. Commun.* **13**, 6140 (2022).
26. G. F. Herrmann, *Phys. Rev.* **133**, A1334–A1344 (1964).
27. D. Treves, *Phys. Rev.* **125**, 1843–1853 (1962).
28. R. Lebrun *et al.*, *Nat. Commun.* **11**, 6332 (2020).
29. M. Białek, J. Zhang, H. Yu, J.-Ph. Ansermet, *Appl. Phys. Lett.* **121**, 032401 (2022).
30. T. Devolder *et al.*, *Phys. Rev. B*. **103**, 214431 (2021).
31. A. H. Morrish, *Canted Antiferromagnetism: Hematite* (WORLD SCIENTIFIC, 1995).
32. R. Lebrun *et al.*, *Commun. Phys.* **2**, 50 (2019).
33. V. Vlaminck, M. Bailleul, *Phys. Rev. B*. **81**, 014425 (2010).
34. Supplementary Material.
35. H. J. Fink, *Phys. Rev.* **133**, 1322–1326 (1964).
36. D. E. Beeman, *J. Appl. Phys.* **37**, 1136–1137 (1966).
37. J. Han *et al.*, *Nat. Nanotechnol.* **15**, 563–568 (2020).
38. I. Boverter *et al.*, *Phys. Rev. Lett.* **126**, 187201 (2021).
39. U. K. Bhaskar, G. Talmelli, F. Ciubotaru, C. Adelman, T. Devolder, *J. Appl. Phys.* **127**, 033902 (2020).
40. J. Cramer *et al.*, *J. Phys. Appl. Phys.* **51**, 144004 (2018).
41. I. V. Rojdestvenski, M. G. Cottam, A. N. Slavin, *Phys. Rev. B*. **48**, 12768–12777 (1993).
42. M. Jamali, J. H. Kwon, S.-M. Seo, K.-J. Lee, H. Yang, *Sci. Rep.* **3**, 3160 (2013).
43. H. Wang *et al.*, Long-distance propagation of high-velocity antiferromagnetic spin waves (2022), , doi:10.48550/arXiv.2211.10989.
44. M. Hamdi, F. Posva, D. Grundler, Spin wave dispersion of ultra-low damping hematite ($\alpha\text{-Fe}_2\text{O}_3$) at GHz frequencies (2022), , doi:10.48550/arXiv.2212.11887.